

Reliable Software Development of a Nanosat Attitude Determination and Control System in a Space-Representative Simulator

Mikel Samson ¹, Rhimas Van de Putte ¹, Wim De Munter ¹, Tjorven Delabie ¹, Andrew Hyslop ², Enrico Melone ²

¹arcsec, firstname@arcsecspace.com, Leuven, Belgium

²ESTEC, firstname.lastname@esa.int, Noordwijk, The Netherlands

INTRODUCTION

The significant growth of the Nanosatellite market is driven by its core advantages: low cost, fast development cycles, and scalability. However, as the market matures and the (scientific) mission potential evolves, the demands for system reliability increase accordingly. The Attitude Determination and Control System (ADCS) is among the most critical systems of a satellite. It provides the pointing functionality and is critical to achieve the mission goals and to keep the satellite in good health. A challenge for performance validation of this system lies in replicating the space environment in simulations and in on-ground test facilities. Furthermore, the low cost and fast development time often drive an incomplete test-campaign, limited to environmental qualification at unit or acceptance test at satellite level. Additionally, the performance is ultimately assessed during on-orbit commissioning, possibly delaying payload operations in case issues need to be resolved.

To bridge the gap between the fast New Space approach and the traditional Guidance Navigation and Control Verification & Validation (GNC V&V) processes, arcsec, a Belgium-based company, started an ESA General Support Technology Program (GSTP) in mid-2024. This paper describes the development work performed in the first phase of the project, where the flight-software is developed and a model-in-the-loop (MIL) performance test campaign is the main output. The ADCS software is developed in MATLAB/Simulink, and accommodates a discrete number of ADCS configurations with varying number of sensors and actuators. Furthermore, it aligns with the SAVOIR autocoding guidelines from ESA to simplify the generation of the C code that can run on the ADCS processor. The usage of code generation also reduces the cost and development time, and ensures traceability between simulations results, hardware-in-the-loop (HIL) tests, and flight data. Furthermore, a list of software requirements is composed which flows down from the system and component level requirements.

In the next sections, the possible configurations and an example design will be discussed. Subsequently, the simulation environment setup for the MIL tests is elaborated. Finally, the last section illustrates some of the results of the MIL simulations in different circumstances.

CONFIGURABILITY

Each mission presents a unique set of requirements that the ADCS must be compliant with. To meet this market demand on diversity, a commercial ADCS must be modular and configurable. Therefore, arcsec's R&D and commercial department conducted a market survey to better understand the range of mission objectives and demands. This survey identified three key criteria that drive the configuration of the ADCS: satellite size, pointing accuracy, and redundancy. Figure 1 shows a diagram with the different configurations that arcsec has determined for each combination of the key criteria. The sections below provide more insight into how each criteria influences the final configuration.

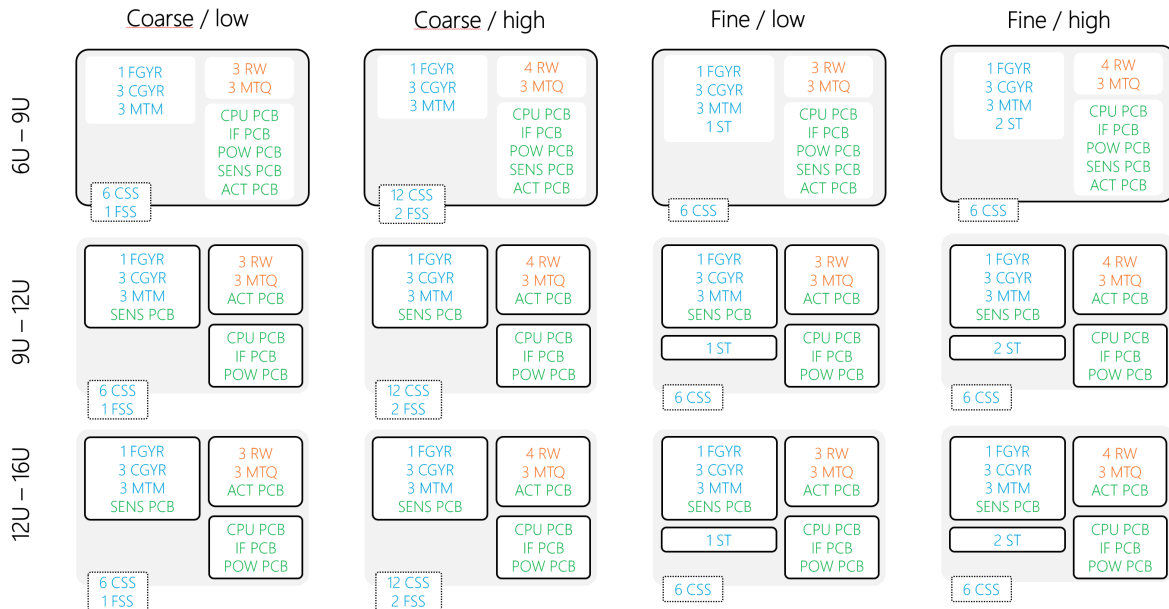


Figure 1: ADCS configurations in function of satellite size (6U to 16U), pointing accuracy (coarse or fine) and redundancy (low or high)

Satellite size

The current ADCS design targets the 6U to 16U CubeSat market, which has become increasingly relevant due to the growing demand for high-performance missions. To address the variation in mechanical and integration constraints across this range, the design is segmented into three satellite size categories: 6U–9U, 9U–12U, and 12U–16U. As the satellite size increases, so do the moments of inertia. To maintain the same level of pointing accuracy in all categories, the actuator configuration must be scaled accordingly. Smaller reaction wheels (RWs) and magnetorquers (MTQs) are used for the 6U-9U category, while for the larger satellites they should deliver respectively more torque and dipole moment. Consequently, this leads to higher power requirements from the actuators, which results in larger electronic components.

On the other hand, the sensor configuration remains invariant in all size categories. Since attitude determination accuracy primarily depends on sensor characterization and calibration rather than spacecraft dynamics, the sensors can be consistently procured across the satellite categories without compromising performance. Lastly, the mechanical configuration also adapts to platform size. In the 6U-9U range, the market requests a single compact unit to minimize volume and ease integration. For larger spacecraft, the ADCS can be split into separate sensor, actuator, and main CPU modules. This provides the integrator more flexible placement, better thermal management and less interference between the actuators and sensors.

Pointing accuracy

The ADCS is configurable to support three categories of pointing accuracy: coarse, fine, and ultra-fine pointing. These modes are defined by the mission’s performance requirements and drive the selection of sensors:

- Coarse pointing targets missions requiring an accuracy of less than 5° (3σ). This level of precision is

typically sufficient for basic orientation, power generation optimization, and low-resolution payload operations. The sensor configuration for this mode includes coarse (CSS) and fine (FSS) sun sensors and magnetometers (MTMs), offering reliable and power-efficient attitude determination.

- Fine pointing improves accuracy to below 0.1° (3σ), suitable for high-resolution imaging, optical communications, or scientific payloads requiring stable line-of-sight control. To meet these requirements, a star tracker is added to the sensor configuration, providing high-accuracy absolute attitude measurements. This significantly enhances the attitude determination accuracy.
- Ultra-fine pointing is intended for missions with even more stringent requirements in the sub-arcminute range. This configuration includes a second star tracker (ST), oriented such that its boresight is perpendicular to the primary tracker. Because a star tracker typically exhibits its highest error around its boresight axis, this orthogonal arrangement allows each tracker to compensate for the other's principal error axis. As a result, the overall attitude determination accuracy improves significantly, especially in dynamic or thermally stressing environments where single-sensor limitations may otherwise dominate.

Redundancy

Redundancy in the configuration ensures that critical system functions remain operational in the event of a single-point failure. This increases mission robustness, can extend operational lifetime, and allows integrators to tailor their system architecture to their specific risk posture. The level of redundancy is configurable based on the mission's reliability requirements and acceptable risk thresholds. For missions with lower criticality or limited resources, a minimal configuration with no hardware redundancy may be sufficient. On the other hand, high-reliability missions with expensive payloads or long-duration deployments can benefit from including redundant units, such as star trackers and reaction wheels.

CUBESPEC ADCS DESIGN

Cubespec is a scientific mission where high-spectral-resolution spectroscopy will be demonstrated in-orbit [2]. The mission is funded by BELSPO, the Belgian federal science policy office and is developed in the ESA GSTP technology programme. Currently, a 12U CubeSat is being designed to accommodate a 10x20 aperture telescope and echelle spectrometer. The spectrometer requires arcsecond-level pointing stability, which should be delivered by a combination of arcsec's ADCS and a high-precision pointing platform (HPPP). The ADCS pointing requirement is $100''$ (3σ) for the cross-boresight axes of the payload, and the HPPP is designed to compensate for the remaining ADCS pointing error. The design of the mission demands high reliability and fine pointing of the ADCS, hence it will include four reaction wheels, three magnetorquers, two star trackers, two ADCS sensor boxes (containing a fine gyroscope (FGYR), three coarse gyroscopes (CGYRs) and three magnetometers) and eight coarse Sun sensors. This sections describes the different modular modules containing the ADCS units as an example configuration.

ADCS Main Module

The ADCS Main Module, shown in Figure 2, is the central unit of the ADCS. It holds the "brain" of the ADCS (i.e. the CPU) and has interfaces to connect to the spacecraft communication bus and power lines and to all ADCS sensors and actuators. Its mechanical design exists of a housing, a side plate and a top plate, with outer dimensions of 94mm x 92mm x 50mm (0.5U) and a mass of approximately 380g.

Furthermore, there are four alignment cut-outs at the bottom and at the top to facilitate the assembly and integration procedure, and four M4 screw holes at the outer corners to fix it to the spacecraft platform. Inside, there are several PCBs to run the control algorithms and manage the power and communication interfaces with the other ADCS modules.

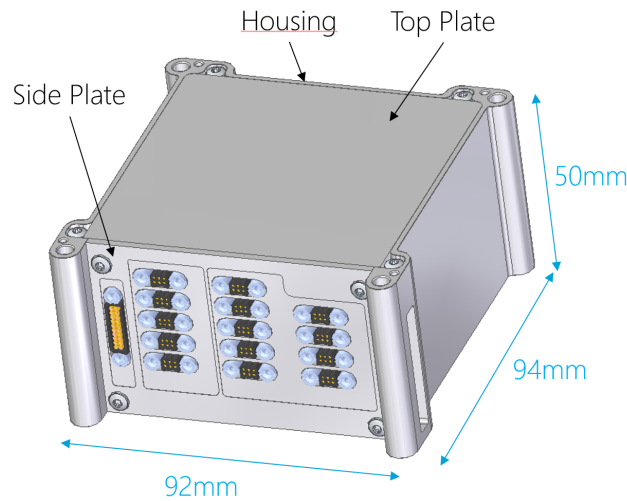


Figure 2: ADCS main module

ADCS Actuator Module

The ADCS Actuator Module, shown in figure 3, contains all actuators, including four reaction wheels and three magnetorquers, as well as their electronics. Its mechanical design exists of a housing, a bracket, and a top plate, with outer dimensions of 94mm x 92mm x 75mm (0.75U) and a mass of approximately 1250g. The ADCS Actuator Module has four alignment cut-outs at the bottom to facilitate the assembly and integration procedure, and has four M4 screw holes at the outer corners to fix it to the spacecraft platform. It also contains separate PCBs for the reaction wheel and magnetorquer electronics.

ADCS Sensor Modules

The ADCS Sensor Module, shown in figure 4a, contains three magnetometers (MTMs), three coarse (MEMS) gyroscopes, and one fine gyroscope. Its mechanical design exists of a housing and a top plate, with outer dimensions of 50mm x 46mm x 20mm (0.05U), a mass of approximately 80g, and has one PCB with all sensors mounted on it. The ADCS Sensor Module has three alignment cut-outs at the bottom and at the top to facilitate the assembly and integration procedure, and has three M3 threaded screw holes at three of the outer corners to fix it to the spacecraft platform. Finally, one M4 screw hole is foreseen at one of the outer corners to allow stacking the ADCS Sensor Module on top of the ADCS Main Module while ensuring fixation to the spacecraft platform.

The ADCS Sun Sensor Module, shown in figure 4b, contains the electronics to connect up to 8 coarse sun sensors, i.e. photodiodes. Its mechanical design exists of a housing and a top plate, with outer dimensions of 46mm x 40mm x 12.5mm (0.02U) and a mass of approximately 50g. It also contains a PCB to interface with all sun sensor electronics and connectors. The ADCS Sun Sensor Module has three alignment cut-outs at the bottom and at the top to facilitate the assembly and integration

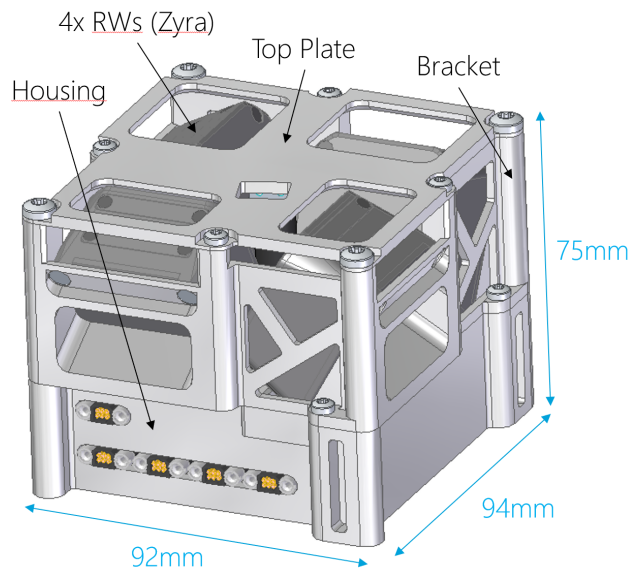
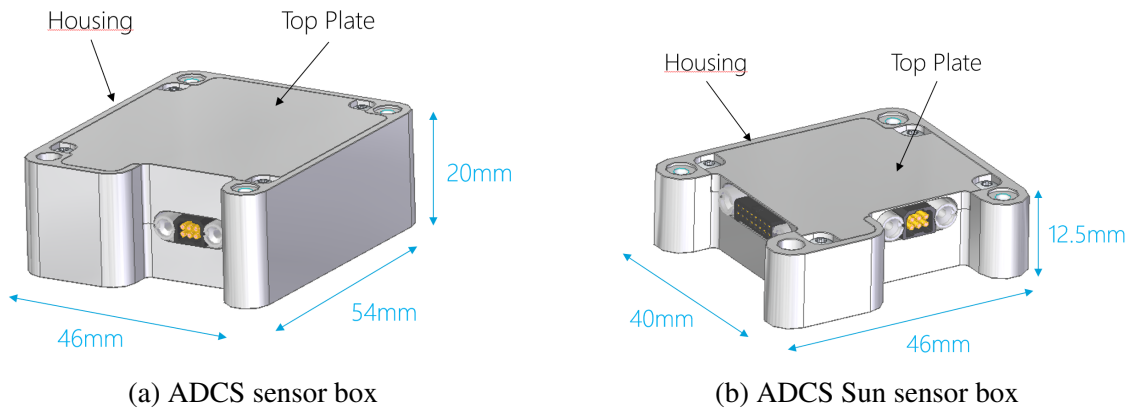


Figure 3: ADCS actuator module

procedure, and has three M3 threaded screw holes at three of the outer corners to fix it to the spacecraft platform. Finally, one M4 screw hole is foreseen at one of the outer corners to allow stacking the ADCS Sun Sensor Box on top of the ADCS Main Box while ensuring fixing to the spacecraft platform.



(a) ADCS sensor box

(b) ADCS Sun sensor box

Figure 4: ESA 3U Cubesat IOD missions flying the arcsec ADCS.

Star trackers

The two star trackers included in the ADCS for the Cubespec mission are the Twinkle and Sagitta, both stand-alone products from arcsec's portfolio. Table 1 lists the characteristics for both star trackers. The attitude determination accuracy of Twinkle is a less performant than Sagitta, but its exclusion angle with baffle is lower. This is a tradeoff between the solution availability and the attitude determination accuracy of the star trackers. Sagitta is mounted with a 20° offset with respect to the payload's boresight axis due to the better accuracy but worse exclusion angle. On the other hand, Twinkle must be oriented alongside the boresight axis to meet the pointing requirement of the mission.

Table 1: Key characteristics of the Sagitta and Twinkle star tracker.

Characteristic	Sagitta	Twinkle	Unit
Full-cone field of view	25.2	10.6	°
Cross-boresight accuracy (1σ)	2	3	"
Along-boresight accuracy (1σ)	10	30	"
Update frequency	10	10	Hz
Power consumption	1.5	0.8	W
Detection magnitude	6.2	7.0	/
Star catalog	6,215	10,000	stars
Focal length	25.2	16.0	mm
Mass	270.0 ± 3	36.0 ± 1.5	g
Size	$95 \times 50 \times 44$	$40 \times 20 \times 20$	mm \times mm \times mm
Half-cone sun exclusion angle (without baffle)	40	80	°
Half-cone sun exclusion angle (with baffle)	30	25	°

SIMULATION ENVIRONMENT

The ADCS flight software is developed in MATLAB/Simulink from which the corresponding C code can be automatically generated for the ADCS processor. The code development aligns with the SAVOIR autocoding guidelines from ESA to simplify the generation of the C code. To assess the performance and reliability of the ADCS flight software, the first phase of the test campaign are model-in-the-loop (MIL) simulations. Therefore, the flight software is linked to an external open-source astrodynamics space environment simulation framework called Basilisk (BSK). BSK is developed jointly by the University of Colorado AVS Lab and the Laboratory for Atmospheric and Space Physics (LASP). The framework is written in C/C++, allowing fast simulation times, and is wrapped to Python for easy interfacing. Within this project, BSK is used to simulate the orbit and attitude of the satellite. Therefore, there is a bidirectional TCP communication channel between MATLAB/Simulink and BSK. An overview of the simulation setup and interfaces is depicted in figure 5. BSK also comes with a visualization tool called Vizard, which allows to visualize the central body, orbit position, attitude, and night sky.

The BSK framework allows to add different modules to the simulation to incorporate all desired elements and effects. The framework has numerous standard modules but also allows to incorporate self-written modules. The following sections describe the different elements which are incorporated in the simulation environment.

Spacecraft Model

The satellite is a rigid body with three translational and three rotational degrees of freedom. The attitude of the spacecraft is determined by the kinematic relation and Euler's rotation equations:

$$\dot{\mathbf{q}} = \frac{1}{2} \boldsymbol{\omega} \otimes \mathbf{q} \quad (1)$$

$$\dot{\boldsymbol{\omega}} = I^{-1} (\mathbf{T} - \boldsymbol{\omega} \times (I\boldsymbol{\omega})) \quad (2)$$

where a dot represents the derivative of a variable or vector, \mathbf{q} represents the attitude quaternion, $\boldsymbol{\omega}$ the angular velocity, I the inertia matrix of the satellite, and \mathbf{T} the torques acting on the satellite. The

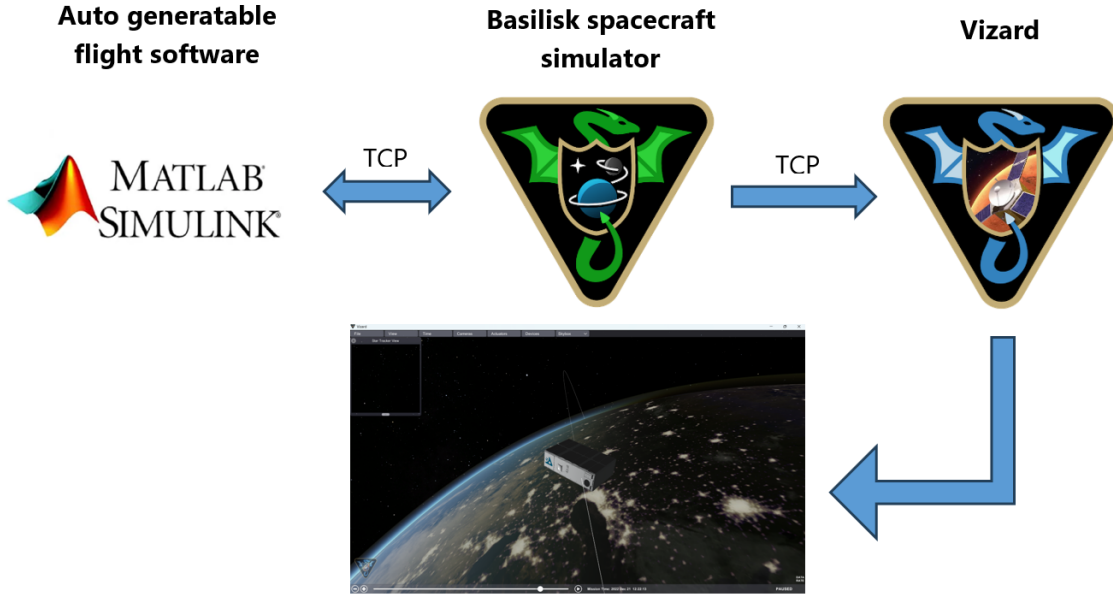


Figure 5: Overview of the simulator setup and interfaces

main focus in the simulations will be attitude maneuvers. Orbital maneuvers will not be considered, and the orbital pose will only be used to determine effects such as disturbance torques, Sun position, Earth position and magnetic field, and eclipse periods.

Environmental Model

Atmospheric Drag

The aerodynamic or drag force vector \mathbf{F}_{aer} for N surfaces i will create an aerodynamic torque \mathbf{T}_{aer} which can be calculated as:

$$\mathbf{T}_{aer} = \sum_{i=1}^N -\mathbf{F}_{aer,i} \times \mathbf{c}_{p,i} = \sum_{i=1}^N \frac{1}{2} \rho C_D \|\mathbf{v}\|^2 S_i (\hat{\mathbf{n}}_i \cdot \hat{\mathbf{v}}) (\hat{\mathbf{v}} \times \mathbf{c}_{p,i}) \quad (3)$$

with $\mathbf{c}_{p,i}$ the center of pressure with respect to its corresponding plane i , ρ the atmospheric density, C_D the drag coefficient, \mathbf{v} the velocity vector in the body frame, S_i the surface area of plane i which the airflow encounters, $\hat{\mathbf{v}}$ the normalized velocity vector in the body frame.

Gravity-Gradient

Since a satellite in Low-Earth-Orbit (LEO) is subjected to the Earth's gravity field, it is subject to a gravity-gradient torque \mathbf{T}_{grav} . This torque is typically formulated as:

$$\mathbf{T}_{grav} = \frac{3\mu}{r^3} (\hat{\mathbf{r}} \times (I \cdot \hat{\mathbf{r}})) \quad (4)$$

where μ is the gravitational parameter of the central body, I is the moment of inertia matrix, \mathbf{r} the position vector from the planet to the spacecraft expressed on the body frame, r the magnitude of \mathbf{r} , and $\hat{\mathbf{r}}$ the normalized position vector.

Solar Radiation Pressure

The solar radiation pressure (SRP) $P(\mathbf{s})$ creates a force \mathbf{F}_{SRP} through satellite surfaces $i = 1 \dots N$. The pressure acting on the spacecraft scaled by the heliocentric distance is calculated as follows:

$$P(\mathbf{s}) = \frac{F}{c} \cdot \left(\frac{U}{\|\mathbf{s}\|} \right)^2 \quad (5)$$

with:

- $F = 1368 \text{ W/m}^2$ the solar radiation flux at 1 astronomical unit,
- $c = 299792458 \text{ m/s}$ the speed of light,
- $U = 149597870700 \text{ m}$ an astronomical unit,
- \mathbf{s} the Sun-relative position vector.

The SRP force acting on the satellite is calculated by summing the SRP force contributions from all N facets:

$$\mathbf{F}_{SRP} = \sum_{i=1}^N -P(\mathbf{s}) S_i \cos(\theta_i) \left[(1 - \delta_i) \hat{\mathbf{s}} + 2 \left(\frac{\rho_i}{3} + \delta_i \cos(\theta_i) \right) \hat{\mathbf{n}} \right] \quad (6)$$

with:

- S_i the surface area of plane i ,
- θ_i the incidence angle between each facet normal vector and the Sun-direction vector,
- δ_i the specular reflection coefficient (fraction of specularly reflected photons),
- ρ_i the diffuse reflection coefficient (fraction of diffusely scattered photons),
- $\hat{\mathbf{n}}$ the facet normal unit vector.

Consequently, the resulting SRP torque \mathbf{T}_{SRP} is calculated as:

$$\mathbf{T}_{SRP} = \sum_{i=1}^N -\mathbf{F}_{SRP,i} \times \mathbf{c}_{p,i} \quad (7)$$

Internal Dipole

The residual dipole of the satellite \mathbf{M}_{res} interacts with the Earth's magnetic field \mathbf{B} and creates a magnetic torque disturbance \mathbf{T}_{mag} :

$$\mathbf{T}_{mag} = -\mathbf{B} \times \mathbf{M}_{res} \quad (8)$$

Sensors & Actuators

The actuator and sensor models are incorporated in the MATLAB/Simulink environment. This offers more flexibility and the existing actuator and sensor models available in BSK are less advanced than the already existing models arcsec has available in MATLAB/Simulink. To maintain the simulation speed of BSK these models would have to be written manually in C/C++ which is not as straightforward since they contain continuous states. The discretization can be taken care of in MATLAB/Simulink takes, which is why these models are implemented there.

Gyroscopes

The ADCS consists of multiple gyroscopes with different measurement accuracies. Although the level of instability is different, all measurements are susceptible to drift over time. Therefore, the introduced bias is modeled by the same widely used gyroscope model given by:

$$\begin{cases} \boldsymbol{\omega}_m = \boldsymbol{\omega} + \boldsymbol{\beta} + \eta_v \\ \dot{\boldsymbol{\beta}} = \eta_u \end{cases} \quad (9)$$

where $\boldsymbol{\omega}_m$ denotes the gyroscope measurement, $\boldsymbol{\beta}$ the gyroscope bias, η_v the gyroscope angular random walk (ARW) and η_u the rate random walk (RRW). The latter two are modeled as additive zero-mean Gaussian noise sequences and depend on the gyroscope type.

Star tracker

The simulation includes a Sagitta and Twinkle star tracker which measure the attitude of the spacecraft via star recognition in captured images. However, if the stray light from the Sun or Earth is too bright or if the rate of the spacecraft is too large, the signal-to-noise ratio of the stars in the image drops and no valid attitude can be determined. Hence, a star tracker measurement cannot be obtained if:

- the Earth is inside the conical exclusion zone, i.e. the angle between the Earth center and the star tracker boresight axis is smaller than the exclusion angle (taking into account the Earth limb),
- the Sun is inside the conical Sun exclusion zone, i.e. the angle between the Sun vector and the star tracker boresight axis is smaller than the exclusion angle,
- the spacecraft rate is above the star tracker rate limit.

Including a full image processing model is too computational expensive for the simulation environment. Therefore, representative Gaussian white noise for the different axes are used with spectral densities corresponding to the datasheet. As the algorithms of the star tracker require a significant computational effort, a delay is introduced between when the image is captured and an attitude solution is returned. Furthermore, a mounting bias, subject to a random walk, is added to the mounting quaternion between the local and body reference frame.

Magnetometer & Sun sensor

The magnetometers and sun sensors are modeled using zero-mean Gaussian noise based on experiments. They do not use advanced models (e.g. the Sun vector is only used to determine the availability of the Sun sensor and not for the noise and also the albedo effect is neglected). However, since these sensors have a low contribution in the presence of multiple star trackers and an accurate gyroscope, this will not significantly affect performance.

Reaction Wheels

The simulation includes four Zyra reaction wheels mounted in a pyramidal configuration. The model of these reaction wheels is obtained by a model-based identification which is performed in former work [1] of the authors. The identified model is a linear frequency-domain model which is extended with non-linear separately-identified effects such as friction and saturation.

Magnetorquers

The magnetorquers are composed of a simple model which adds some quantified zero-mean Gaussian noise to the requested dipole moment. Furthermore, the residual dipole of the MTQs after deactivation is included in the simulation. This residual dipole does not only affect the satellite's attitude, but it also disturbs the MTM measurements (when the MTQs are deactivated). The measured magnetic field disturbance B_{MTQ} of the residual dipole \mathbf{m} is calculated as:

$$\mathbf{B}_{MTQ} = \frac{\mu_0}{4\pi} \left(\frac{4\mathbf{r}(\mathbf{r} \cdot \mathbf{m})}{r^5} - \frac{\mathbf{m}}{r^3} \right) \quad (10)$$

where μ_0 denotes the vacuum permeability, \mathbf{r} the position vector from the MTQ to the MTM, and \mathbf{m} , and r the magnitude of \mathbf{r} .

SIMULATION RESULTS

Nadir Pointing

A common pointing mode for an ADCS is nadir pointing where one face is directed towards the Earth's surface. Figure 6 shows the disturbance torque acting on the satellite obtained by a simulation of one orbit in a nadir pointing mode. Because one face is perpendicular to the Earth's surface and hence parallel to the gravitational force, the gravity gradient torque is constant. To constrain the other degrees of freedom of the attitude, a second face is optimally pointed along the velocity vector of the orbit. The aerodynamic and magnetic torque vary with an orbital period as a result of the varying attitude and magnetic field. The SRP torque is nearly constant since the combination of the orbit and pointing mode cause the Sun vector in the body frame of the satellite to be almost constant. This can also be seen in figure 7 which shows the angles between two star trackers and the Earth and Sun. Additionally, the dotted lines indicate the Earth and Sun exclusion angles of the STs. Due to the nadir pointing mode, the angles between the Earth vector and the boresight axes of the STs are constant. The angle with respect to the Sun vector is also nearly constant. Since the mounting angle between the STs is equal to 20° , there is a small difference between the two STs. On the right, figure 7 also shows the actual angular rate of the satellite, which never exceeds the threshold resulting in continuous solution availability of the STs.

As illustrated in figure 8, the RW angular velocities vary throughout the orbit to compensate the disturbances and nutation torques. However, the RWs torques are not only compensating the disturbances. The active momentum control of the RWs by the MTQs and null-space control among the RW array will change the RW velocities without affecting the total momentum of the satellite. The algorithms drive the RW velocities to ± 1000 RPM to avoid zero-crossings. Because the initial velocities of the RWs deviate from the desired, the momentum and null-space control will drive them to the desired velocity which can be seen by the steep slope in the beginning. Afterwards, the variations are a combinations of disturbance compensation and switching to another momentum distribution among the array.

Figure 9 shows the resulting pointing error of the ADCS for the three Euler angles in time and as a cumulative error. The error shows a zero steady-state error and similar performance for all three axes. Table 2 lists the corresponding 1σ , 2σ , and 3σ bounds of the estimation, control, and total error. The estimation error on the yaw axis is significantly larger than the roll and pitch axes since the boresights of the STs are more or less aligned with the yaw axis. The control error on the other hand is similar in the three axes, as the controller gains are tuned to achieve uniform bandwidth on each axis. The

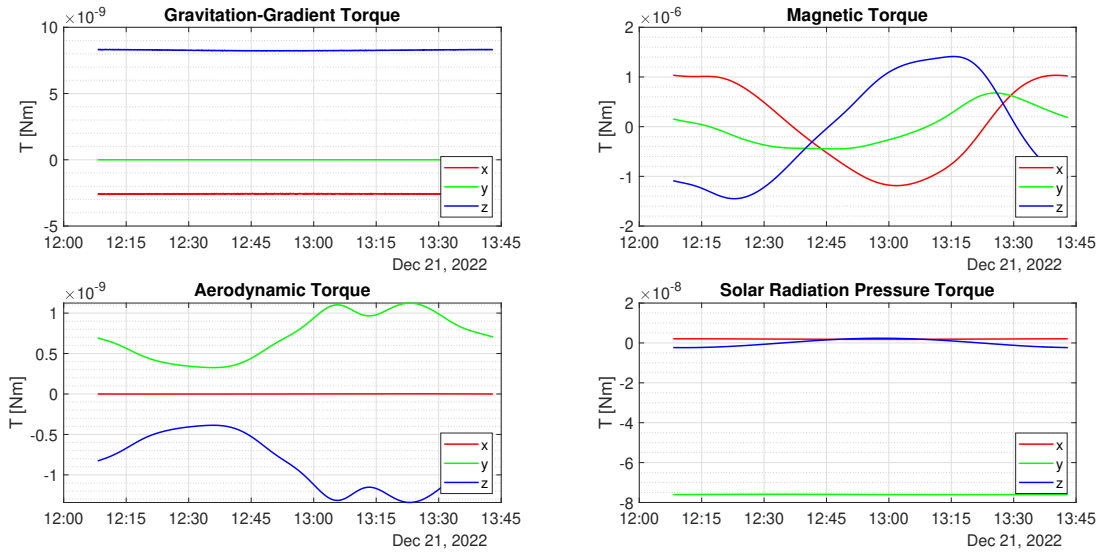


Figure 6: Disturbance torque in nadir pointing for one orbit

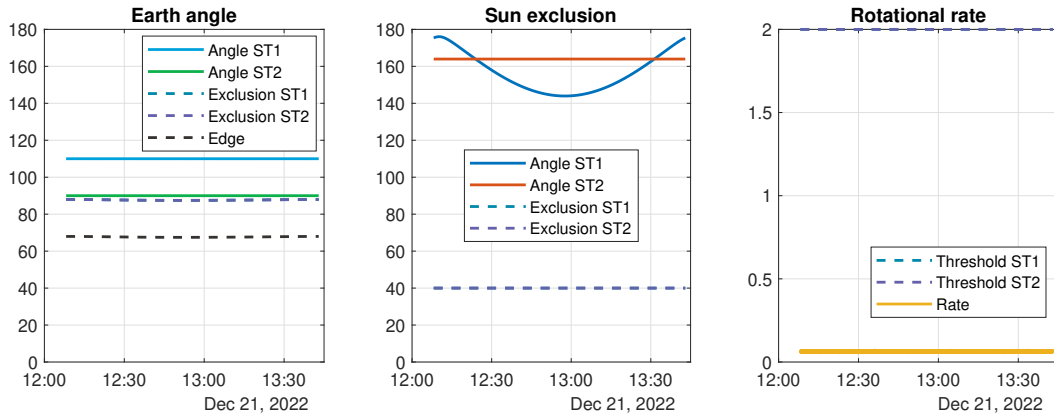


Figure 7: ST exclusion angles & availability in nadir pointing for one orbit

close similarity between the control error and the total error indicates the control error is the primary contributor to the total pointing error.

Table 2: Sigma-bounds of the estimation, control, and total error in the nadir pointing for one orbit

	1σ			2σ			3σ		
	Roll	Pitch	Yaw	Roll	Pitch	Yaw	Roll	Pitch	Yaw
Estimation	1.668	1.285	3.215	3.027	2.547	6.35	4.336	3.897	9.706
Control	9.504	9.086	9.233	18.98	17.64	18.28	30.22	27.14	30.40
Total	9.504	8.993	9.018	18.91	17.48	17.76	30.05	26.59	30.31

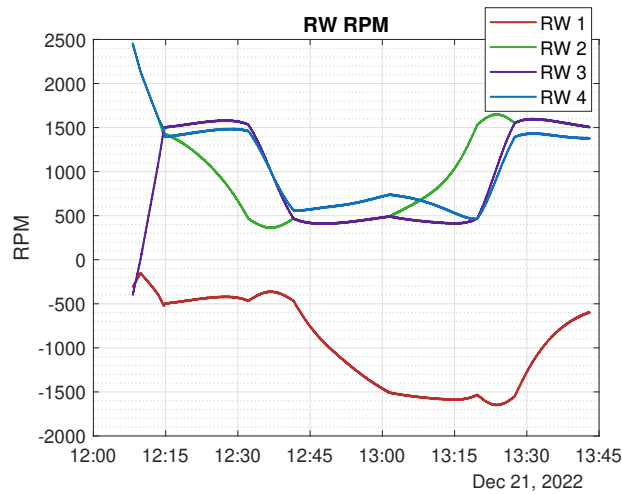


Figure 8: RW velocities in nadir pointing for one orbit

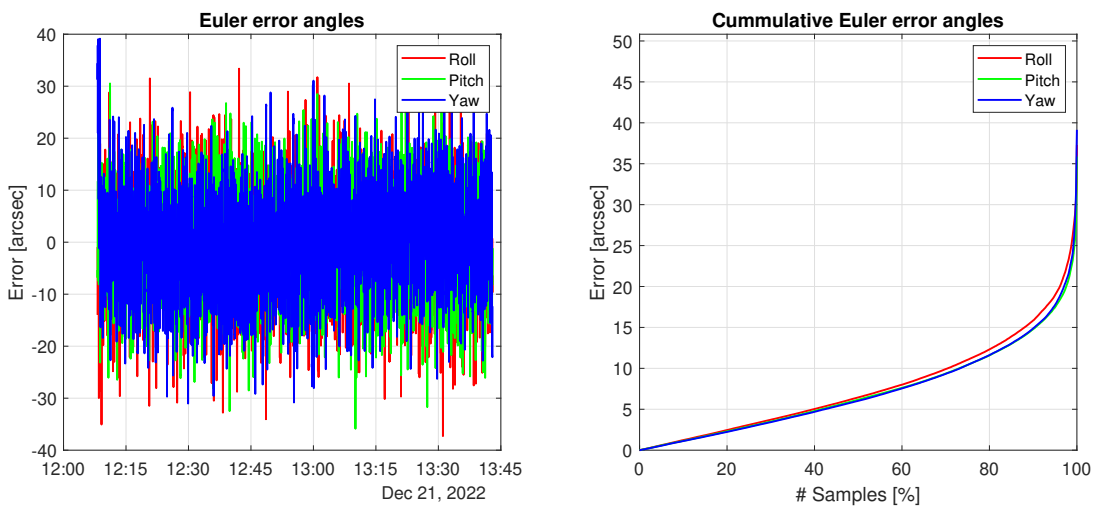


Figure 9: Euler angle errors in nadir pointing for one orbit

Slew maneuvers

Some missions require the satellite to perform rapid slew maneuvers when the observation target varies in time. One example is the CubeSpec ESA IOD mission scheduled to be launched in 2026. This mission will require four to six slews per orbit, and hence requires a rapid settling time to maximize the observation time. Figure 10 illustrates six representative slew maneuvers throughout one orbit. The slew time and settling time are also depicted for each slew in the figure. They represent the time before the overall error is smaller than respectively 5% and 0.1%. The slews are performed such that the maximal rate of $2^\circ/s$ is not exceeded to maintain the star tracker availability. It can be seen that for a variation of slew angles, the overshoot and the settling time after the constant rate trajectory are similar.

Figure 11 shows the angular velocities of the RWs to perform the six slew maneuvers. Despite the momentum and null-space control, zero-crossings cannot always be avoided. However, they do not significantly affect the pointing performance.

Figures 12 and 13 show the Sun and Earth angles and the exclusion angles of the star tracker. The

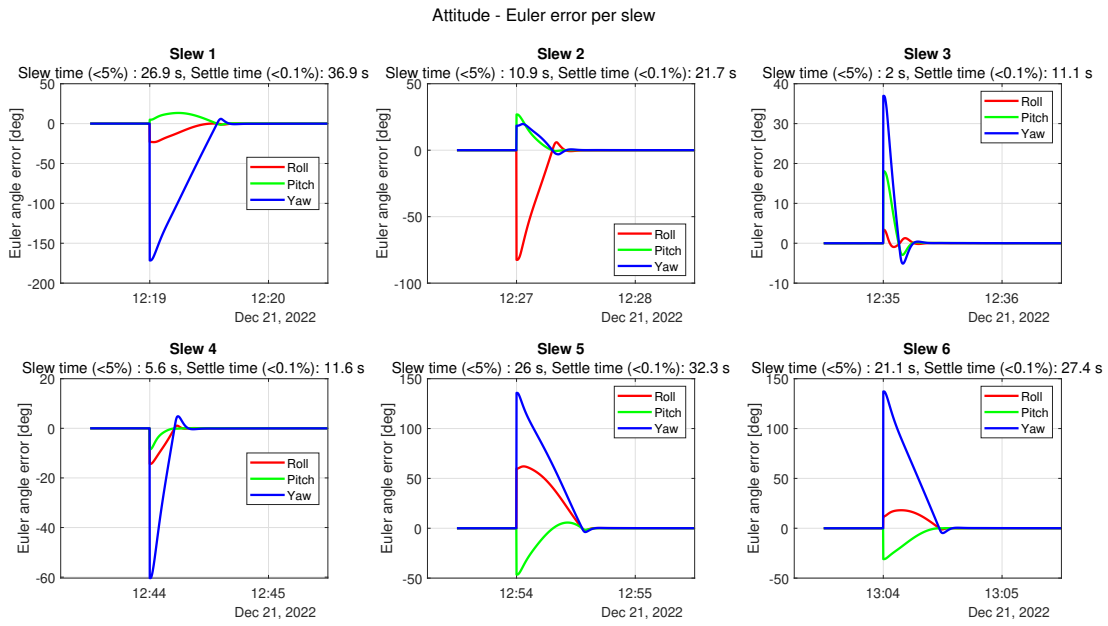


Figure 10: Euler angle errors during six slew maneuvers

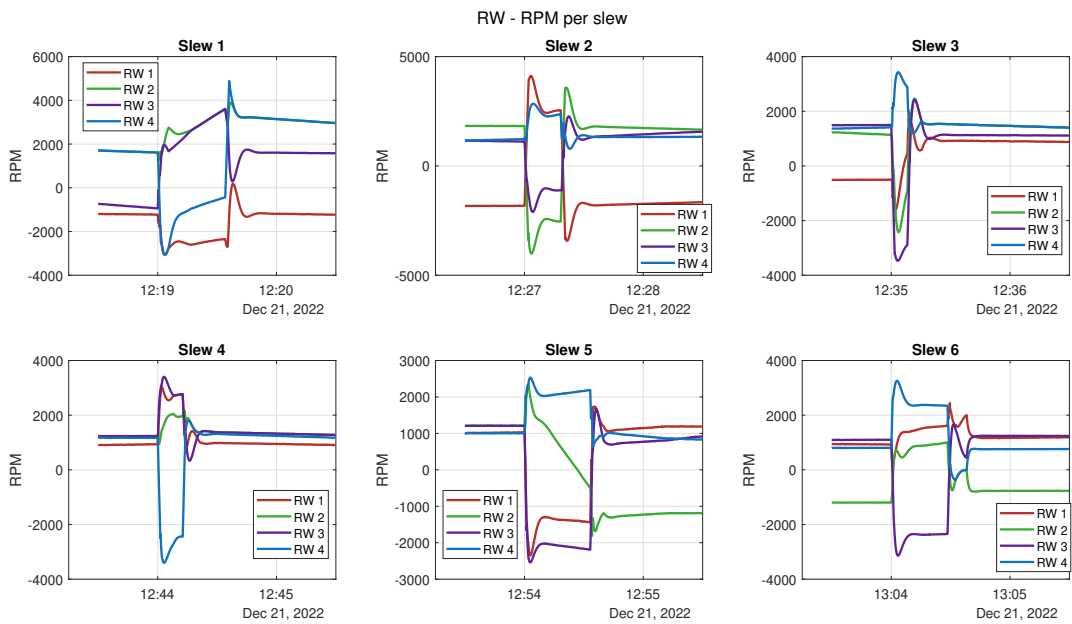


Figure 11: RW velocities during six slew maneuvers

time violation with respect to the exclusion angles is also depicted. For most of the slews, there are no violations. However, for some slews, there is a violation during the slew, which will lead to temporary unavailability of the star tracker.

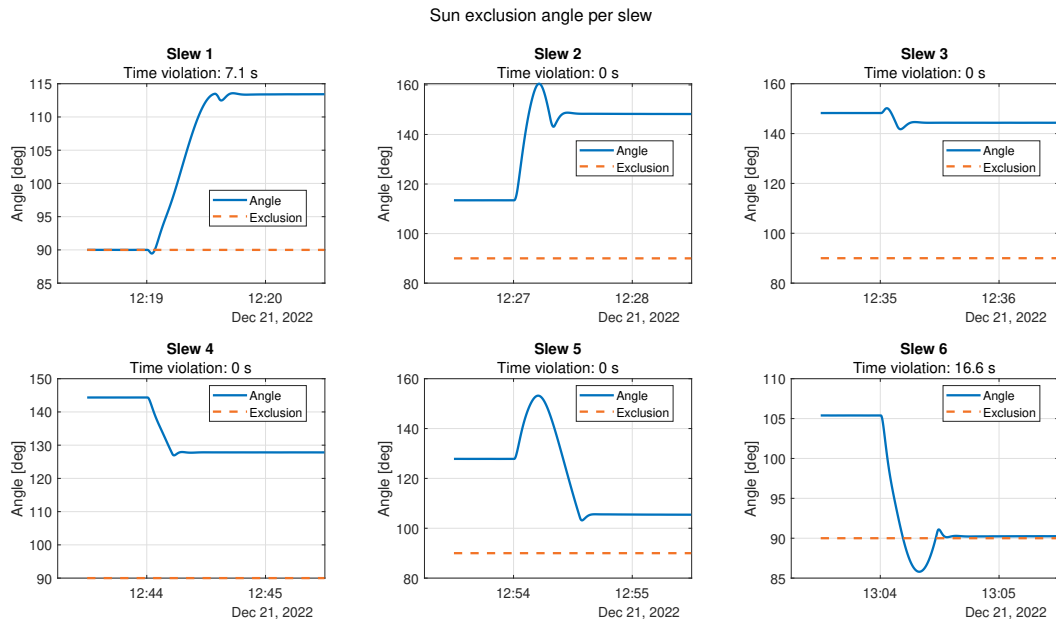


Figure 12: ST Sun exclusion angle during six slew maneuvers

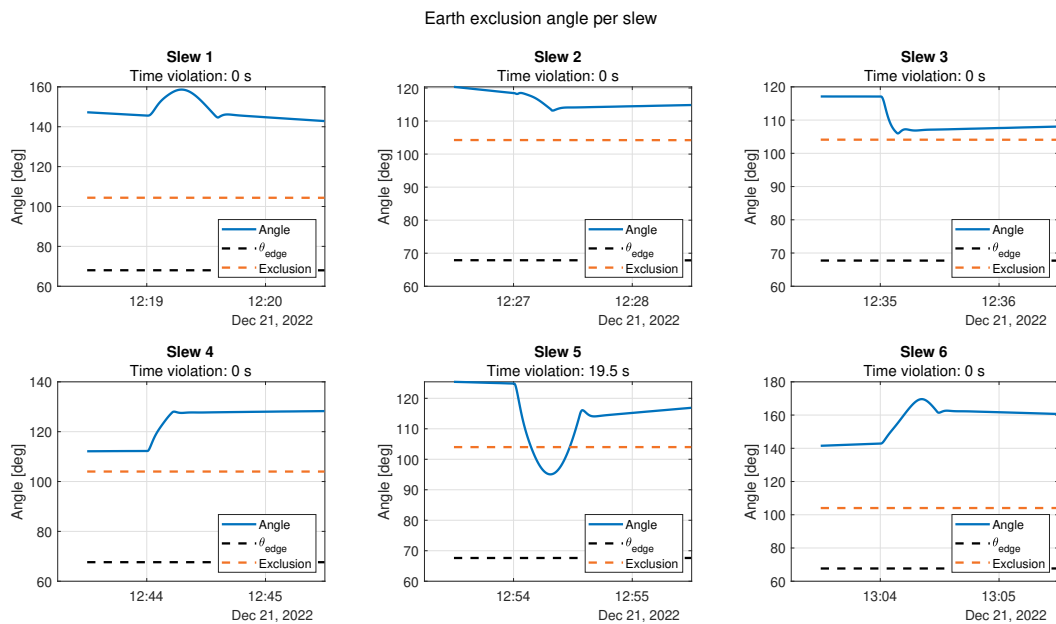


Figure 13: ST Earth exclusion angle during six slew maneuvers

CONCLUSION

This paper presents the design of a modular and configurable Attitude Determination and Control System (ADCS) that is being developed by arcsec. Its properties ensure that the ADCS can accommodate a whole range of requirement sets that is demanded by the market. Therefore, three key criteria were

identified which drive the ADCS configuration: satellite size, pointing accuracy, and redundancy. The former criterion drives the actuator selection, as the inertia and hence the torque requirements are scaled accordingly. The sensor configuration primarily determines the pointing accuracy: coarse pointing only relies on magnetometer and Sun sensors, while the fine pointing requires at least one star tracker to reach $< 0.1^\circ$. Ultra-fine pointing targets sub-arcminute accuracy, for which at least 2 star trackers are required with their boresight axes perpendicular to each other. Redundancy of the most critical units provides mission robustness and possible extension of the operational lifetime of the mission in the event of a single-point failure.

The simulation environment which is used to verify the performance, is based on the external open-source astrodynamics space environment simulation framework called Basilisk. It provides the satellite and environmental models, including the dynamic and kinematic equations, and disturbance torques acting on the satellite from the atmospheric drag, the gravity-gradient, the solar radiation pressure, and the internal dipole moment. The models for the actuators are included in the MATLAB/Simulink part of the Model-in-the-Loop simulation environment and are based as much as possible on experimental data.

This environment allows to simulate realistic pointing scenarios for the Cubespec mission, a 12U Cube-sat for which the ADCS should deliver $100''$ (3σ) on the cross-boresight axes of the payload. For a nadir pointing mode, one face always points to the Earth's surface, leading to a constant gravity-gradient torque. The aerodynamic, magnetic and SRP torque vary with an orbital period. However, as the pointing mode results in an almost constant Sun vector, the variation on the SRP torque is almost constant. The RW angular velocities are varying to compensate these disturbance torques. The null-space of the RW array and the momentum control of the MTQs are attempting to drive these velocities to a desired velocity while avoiding zero-crossings. The resulting pointing error shows a zero-steady state and similar performance for all three axes. The estimation error accounts for 20%-30% of the total error, while the contribution of the control error is significantly higher. Slew maneuvers between different observation targets are performed such that the maximal slew rate of the star trackers are not exceeded to maintain solution availability. The trajectory tracking results in similar overshoot and settling times for a variation of slew angles.

FUTURE WORK

Future activities include the assembly, integration, and environmental testing of the ADCS developed for the CubeSpec mission. At the time of writing, launch is planned for mid-2026. In parallel, a second engineering model (EM) is being developed under the GSTP project, with a comprehensive verification and validation (V&V) campaign scheduled for the second half of 2025. This campaign will involve unit-level performance testing of the most critical components, i.e. the reaction wheels, gyroscopes, and star trackers. Additionally, the engineering model will undergo system-level hardware-in-the-loop (HIL) testing on a three-degree-of-freedom air bearing platform.

REFERENCES

- [1] R. Van de Putte, M. Samson, L. Kazemi, and T. Delabie. Model-based control of a novel outrunner reaction wheel for cubesats and smallsats. In *AIAA SCITECH 2024 Forum*, page 1258, 2024.
- [2] B. Vandenbussche, G. Raskin, H. Sana, D. Vandepitte, J. De Maeyer, P. Royer, L. Peri, A. Tkachanko, S. Van Gool, J. Windey, P. Neuville, D. Bowman, J. Morren, J. Pember, M. Reggiani, W. De Munter, M. Kempnaers, B. Vandoren, and T. Delabie. The CubeSpec mission: high

resolution spectroscopy from a CubeSat. In L. E. Coyle, S. Matsuura, and M. D. Perrin, editors, *Space Telescopes and Instrumentation 2024: Optical, Infrared, and Millimeter Wave*, volume 13092 of *Society of Photo-Optical Instrumentation Engineers (SPIE) Conference Series*, page 1309206, Aug. 2024.